Robust Transceiver to Combat Periodic Impulsive Noise In Narrowband Powerline Communications

Jing Lin*, Tarkesh Pande†, Il Han Kim†, Anuj Batra† and Brian L. Evans*
*Wireless Networking and Communications Group, The University of Texas at Austin, Austin, TX 78712 USA
†Texas Instruments, Dallas, TX 75243 USA

***Abstract*—Non-Gaussian noise/interference severely limits communication performance of narrowband powerline communication (PLC) systems. Such noise/interference is dominated by periodic impulsive noise whose statistics varies with the AC cycle. The periodic impulsive noise statistics deviate significantly from that of additive white Gaussian noise, thereby causing dramatic performance degradation in conventional narrowband PLC systems. In this paper, we propose a robust transmission scheme and corresponding receiver methods to combat periodic impulsive noise in OFDM-based narrowband PLC. Towards that end, we propose (1) a time-frequency modulation diversity scheme at the transmitter and a diversity demodulator at the receiver to improve communication reliability without decreasing data rates; and (2) a semi-online algorithm that exploits the sparsity of the noise in the frequency domain to estimate the noise power spectrum for reliable decoding at the diversity demodulator. In the simulations, compared with a narrowband PLC system using Reed-Solomon and convolutional coding, whole-packet interleaving and DBPSK/BPSK modulation, our proposed transceiver methods achieve up to 8 dB gains in E_b/N_0 with convolutional coding and a smaller-sized interleaver/deinterleaver.**[1]

I. Introduction

Powerline communication (PLC) is a technology that enables sending data over electric power lines. Thanks to the widespread availability of power line infrastructure, PLC has been considered as a low-cost solution for smart grid communications. In particular, narrowband PLC operating in the 3–500 kHz band has gained tremendous interest for enabling communications between smart meters and data concentrators that are deployed by local utilities on low-voltage or medium-voltage power lines [2]. The applications include automatic meter reading, device-specific billing, time-dependent pricing and other real-time control and monitoring. Examples of narrowband PLC systems are specified in standards such as ITU-T Recommendations G.9903 [3] and the IEEE 1901.2 standard [4]. These standards use Orthogonal Frequency Division Multiplexing (OFDM) to deliver scalable data rates up to several hundred kbps over a portion of the European CENELEC band (3–95 kHz in CENELEC-A, 95–125 kHz in CENELEC-B and 125–148.5 kHz in CENELEC-CD) and the entire US FCC band (34.375-487.5 kHz).

One of the primary challenges for narrowband PLC is to overcome additive powerline noise. Recent field measurements on both indoor and outdoor power lines have identified the dominant noise component in the 3–500 kHz band to be periodic impulsive noise [5], [6], [7], whose statistics varies periodically with half the AC cycle. Such noise exhibits cyclostationarity in both time and frequency domain (Fig.1). In general, it is comprised of two impulsive noise components, whose impulse rates are either synchronous or asynchronous to the main powerline frequency. The synchronous periodic impulsive noise consists of isolated impulses with a repetition rate equal to twice the main powerline frequency. On the other hand, the asynchronous periodic impulsive noise takes the form of bursts that occur twice per AC cycle. Each burst consists of an impulse train whose impulse rates are unrelated to and much higher than the main powerline frequency. The periodic structure within each impulse train results in a sparse power spectral density where the noise power is concentrated around a few frequency components, similarly to that of narrowband interference. A primary contributor to the asynchronous periodic impulsive noise is switching mode power supplies, such as inverters and DC-DC converters, which contain MOSFET switches operating at frequencies above 20 kHz and up to several hundred kHz. These circuits output inband harmonic contents that cannot be perfectly removed by analog filtering.

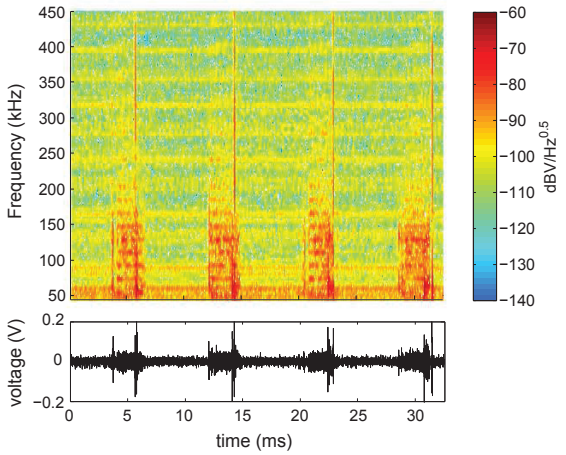

Fig. 1. Spectrogram (top) and time-domain trace (bottom) of an example periodic impulsive noise trace measured from an outdoor low-voltage site [5].

Several statistical models have been suggested in the literature to capture the temporal and spectral properties of the periodic impulsive noise [5], [6]. A linear periodically time varying (LPTV) system model was proposed in [5] and later adopted by the IEEE 1901.2 narrowband PLC standard. The model was established on the approximation that each period of the noise can be partitioned into a number of intervals, and that within each interval the noise is a stationary Gaussian process characterized by a particular power spectral density. For example, the noise trace in Fig. 1 can be modeled as a

[1]This work was supported by gift funding and equipment donations from National Instruments, as well as grant funding from the Semiconductor Research Corporation under Task ID 1836.133 with liaisons Freescale Semiconductor and Texas Instruments. An extended version of this work is under review for publication in IEEE Transactions on Communications [1].

cyclostationary Gaussian process where each period consists of three stationary intervals. The third stationary interval is comprised of wideband impulsive noise synchronous to the main powerline frequency. The first two contain periodic impulsive noise asynchronous to the main powerline frequency, which can be identified from the sparse power spectral densities.

In addition to the periodic impulsive noise, PLC systems within a smart grid network also suffer from uncoordinated interference from neighboring PLC devices. Such interference is generally characterized by asynchronous impulsive noise [5], which consists of high amplitude impulses that occur randomly in time. In this work, we focus on combating periodic impulsive noise, and assume that the uncoordinated interference from neighboring PLC devices has either been avoided by co-existence mechanism [2], or mitigated at the receiver using pre-processing methods [8].

Prior work to combat periodic impulsive noise in OFDM systems involves efforts from both the transmitter and receiver's perspectives. Transmitters specified in existing narrowband PLC standards [3], [4] rely on forward error correction coding and frequency-domain block interleaving to cope with impulsive noise. In particular, it was suggested to use concatenated forward error correction codes (i.e., convolutional, Reed-Solomon and repetition codes) to enhance the error correction capability in harsh channel and noise environments. Heavy coding, however, sacrifices throughput (or equivalently, requires bandwidth expansion) for improved reliability. On the receiver side, pre-processing algorithms were developed to mitigate the impact of periodic impulsive noise. Some receiver methods estimated the second-order cyclostationary noise statistics by training, and designed parametric filters for noise whitening [9], [10], [11]. Others used time-domain block interleaving to spread a noise burst into scattered impulses [12], and estimated the impulses from received signal by exploiting its sparsity in time domain [8].

In this work, we aim at improving reliability of OFDM-based narrowband PLC systems in periodic impulsive noise without reducing throughput. Towards that end, we adopt modulation diversity [13] and propose a time-frequency modulation diversity technique that exploits the channel diversity provided by the periodically varying and spectrally shaped noise. An attractive feature of modulation diversity, compared to other diversity schemes, is that it does not incur data rate reduction or bandwidth expansion [13]. To improve the robustness of the diversity combining receiver, we propose a semi-online noise power spectrum estimation algorithm that iteratively infers noise power spectrums from received signal, while partially relying on noise measurements prior to transmission.

Compared to previous studies, our proposed transceiver methods have several advantages. Unlike concatenated forward error correction coding, our transmission scheme using modulation diversity does not decrease data rates for improved robustness. As will be demonstrated by simulation results, our proposed system outperforms conventional narrowband PLC system with Reed-Solomon coding, while eliminating the enormous complexity of Reed-Solomon decoding. Furthermore, the proposed transceiver methods can be easily integrated into existing narrowband PLC standards. In particular, it does not depend on time-domain interleaving, which is an essential element in [8], [12] but is not standard-compliant. Finally, the proposed semi-online noise power estimator is primarily data-driven, and saves significant training overhead compared to the parametric noise mitigation methods [9], [10], [11].

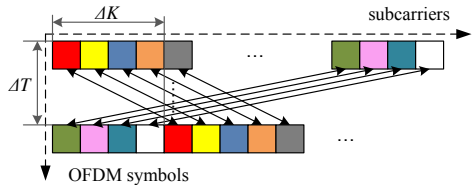

Fig. 2. An example of time-frequency modulation diversity. The two components of a codeword (marked in the same color) are allocated to subcarriers i in OFDM symbol j, and subcarrier $\big((i+\Delta K) \mod N_{\text{data}}\big)$ in OFDM symbol $\big((j+\Delta T) \mod N_{\text{OFDM}}\big)$, $\forall i, j$, where N_{data} is the number of data subcarriers in an OFDM symbol, and N_{OFDM} is the number of OFDM symbols in a packet.

II. Time-Frequency Modulation Diversity

Modulation diversity has been used in the literature to improve communication reliability by spreading information over multiple sub-channels and hence exploiting channel diversity. Several categories of modulation diversity codes have been investigated [13], [14], [15], [16], among which the Hochwald/Sweldens codes have attracted a lot of attention [16]. A Hochwald/Sweldens codebook defines a one-to-one mapping from any group of N_dR bits to an N_d dimensional constellation point, each dimension of which is a phase shift keying (PSK) symbol:

$$f : \mathbf{c} \in \{0,1\}^{N_dR} \rightarrow \mathbf{s} \in \mathcal{C}^{N_d}. \tag{1}$$

Here R denotes the original data rate in bits per symbol, and $\mathcal{C}$ denotes a 2^{N_dR}-PSK constellation. Note that the same data rate of R is maintained after modulation diversity, if the N_d components of $\mathbf{s}$ are transmitted over different sub-channels. The n-th component of a codeword $\mathbf{s}^{(m)}$ has the form

$$s_n^{(m)} = \exp(j2\pi u_n m/2^{N_dR}), \tag{2}$$

$\forall m = 1, \cdots, 2^{N_dR}$, $\forall n = 1, \cdots, N_d$. When $u_n = 1, \forall n$, the Hochwald/Sweldens code reduces to a PSK repetition code [13]. Assuming that all components of a codeword are transmitted over static flat channels or $i.i.d.$ flat Rayleigh fading channels and corrupted by AWGN, the optimal values of $\mathbf{u}$ for $R = 1$ and $N_d = 2$ to 4 have been found by exhaustive search [16]. The Hochwald/Sweldens codes can be easily integrated into most existing narrowband PLC standards, which adopt PSK as a modulation scheme.

In OFDM-based narrowband PLC systems, recognizing the periodically varying spectrally shaped statistics of periodic impulsive noise, we propose to apply modulation diversity across time and frequency, which leads to the time-frequency modulation diversity (TFMD). In TFMD, components of a modulation diversity codeword are transmitted on various subcarriers in multiple OFDM symbols. To achieve better performance, such time-frequency mapping needs to be configured properly according to the burst structure of the noise and the OFDM parameters. A simple mapping scheme is depicted in Fig. 2, assuming $N_d = 2$ as an example. In general, the N_d components of a modulation diversity codeword are spread into time and frequency units so that adjacent components are separated by ΔK subcarriers and ΔT OFDM symbols. To reduce the possibility that all components are affected by narrowband

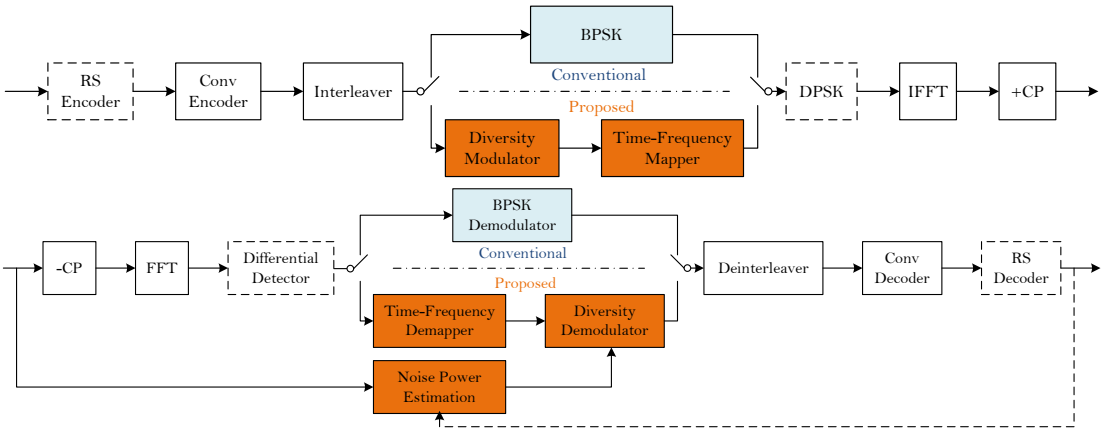

Fig. 3. A conventional OFDM narrowband PLC transmitter (top) and receiver (bottom), compared to the proposed transmitter and receiver using time-frequency modulation diversity. The dashed blocks, i.e., the Reed-Solomon (RS) encoder/decoder and differential (DPSK) encoder/detector, can be optionally switched on and off. In non-coherent mode, the noise power spectrums can be estimated before transmission. In coherent mode, it can also be estimated iteratively using a semi-online method, using decision feedback from the decoder.

interference or a deep fade in frequency domain, we divide the transmission band evenly into N_d subbands, and distribute the components in different subbands, i.e., $\Delta K = N_{\text{data}}/N_d$, where N_{data} denotes the number of data subcarriers in an OFDM symbol. Likewise, to ensure that not every component of a codeword is contaminated by noise bursts, ΔT is set to be the maximum number of consecutive OFDM symbols in a single noise burst. Thanks to the cyclostationary property of the noise, the burst duration within a period of the noise can be pre-determined by the receiver and made available to the transmitter via receiver feedback.

The block diagram for an OFDM-based narrowband PLC transmitter using TFMD is shown on the top of Fig. 3 and compared with a conventional transmitter operating in DBPSK/BPSK mode, using similar physical layer specifications as in the ITU-T G.9903 standard. The transmitters can be configured to operate in either of the two transmission modes: non-coherent (i.e., differential) and coherent. In a non-coherent system, a reference OFDM symbol is inserted at the beginning of a packet, upon which the following symbols are differentially encoded in the time domain. Our proposed transmitter is built upon the conventional transmitter, by replacing the BPSK modulator with the TFMD modulator. More specifically, the TFMD modulator is comprised of a diversity modulator that maps every N_d bits to N_d PSK symbols, and a time-frequency mapper that allocates the PSK symbols to N_d designated time-frequency units. Note that TFMD itself does not change the data rates (in bits per sub-channel).

A diversity demodulator combines received signal in N_d time-frequency slots to generate soft decisions on the N_d bits. Such combining depends on the estimation of the periodically varying noise power spectral density. Consider a group of bits, $\mathbf{c} \in \{0,1\}^{N_d}$, that is jointly mapped to a modulation diversity codeword. Suppose that the n-th component of the codeword is allocated to subcarrier i_n in the j_n-th OFDM symbol, $\forall n = 1, \cdots, N_d$, which is denoted by $v_{i_n j_n}$. To simplify notations, define index sets $I \triangleq \{i_n\}_{n=1}^{N_d}$ and $J \triangleq \{j_n\}_{n=1}^{N_d}$, and a column vector $\mathbf{v}_{IJ} \triangleq \{v_{i_n j_n}\}_{n=1}^{N_d}$. The soft decisions on $\mathbf{c}$ consists of N_d log-likelihood ratios (LLRs), one for each bit. In non-coherent systems, the LLRs are conditioned on the received signal $\mathbf{r}_{IJ}$ and the reference signal $\mathbf{r}_{I,J-1}$, and can be derived as [1]

$$L(c_n) = \max_{\mathbf{v}_{IJ}:c_n=0} \sum_{k=1}^{N_d} \frac{\text{Re}\{r_{i_k j_k} v_{i_k j_k}^* r_{i_k, j_k-1}^*\}}{\tilde{\sigma}_{i_k j_k}} - \max_{\mathbf{v}_{IJ}:c_n=1} \sum_{k=1}^{N_d} \frac{\text{Re}\{r_{i_k j_k} v_{i_k j_k}^* r_{i_k, j_k-1}^*\}}{\tilde{\sigma}_{i_k j_k}}. \quad (3)$$

where $\tilde{\boldsymbol{\sigma}}_{IJ} = \boldsymbol{\sigma}_{I,J-1} + \boldsymbol{\sigma}_{IJ}$, and $\sigma_{i_n j_n}$ is the noise variance in the corresponding time-frequency slot. Compared to conventional DPSK detection, the diversity demodulator (3) combines the decision metrics from N_d time-frequency slots, with the weights inversely proportional to the noise variances.

Following similar derivations, it can be verified that the diversity demodulator for coherent systems take the same mathematical form as (3), except for replacing the reference signal r_{i_k, j_k-1} with the channel estimation $\hat{h}_{i_k j_k}$, and $\tilde{\sigma}_{i_k j_k}$ with $\sigma_{i_k j_k}$. The bottom of Fig. 3 depicts the modulation diversity receiver that takes into account of the cyclostationary noise statistics, compared with a conventional OFDM receiver assuming AWGN.

III. Noise Power Estimation

Performance of the diversity demodulator depends on the accuracy of noise power estimation. Such estimation can be done offline, where the receiver collects noise samples that span multiple AC cycles before the transmission starts, and uses that to estimate noise power spectrums. More specifically, it takes a short time Fourier transform (by sliding FFT) over the recorded noise samples, and averages the instantaneous noise power spectrums in each stationary interval. Within a smart grid network, PLC transmissions from different devices need to be scheduled using multiple access protocols (e.g. carrier sense multiple access) to limit uncoordinated interference [2]. As the number of PLC devices increases, the length of idle intervals, when none of the devices is transmitting, becomes limited. In this situation, a receiver might not be able to collect sufficient noise samples to make accurate noise power estimation, or more advanced techniques have to be used to discriminate powerline noise from transmissions by neighboring devices. Therefore, it is desirable to develop algorithms to estimate noise power spectrums primarily during data transmission.

Towards that end, we present a semi-online algorithm to estimate the noise power spectrums in the stationary intervals that have a sparsity noise power spectral density. Signal received in other stationary intervals is generally overwhelmed by high power noise (e.g. the third stationary interval in Fig. 1), and has negligible contribution to the LLR computation in (3). Therefore, we can simply discard the signal received in this type of stationary intervals, without estimating the noise power.

Let N_c and N_p denote the FFT size and CP length in an OFDM system, and L_h the channel delay spread in samples. Most narrowband PLC standards adopt a CP that is much longer than typical channel delay spreads (i.e., $N_p \gg L_h$) [5]. The first L_h samples inside the CP are affected by inter-symbol-interference. Removing these samples from the j-th received OFDM symbol in time domain results in

$$\dot{\mathbf{r}}_j = \mathbf{H}_j \mathbf{S} \mathbf{F}_{N_c}^* \mathbf{s}_j + \dot{\mathbf{e}}_j.$$

Here $\mathbf{F}_{N_c}$ is the N_c-point FFT matrix, $\mathbf{S} \triangleq \begin{bmatrix} \mathbf{0}_{N_c-N_p+L_h} & \mathbf{I}_{N_p-L_h} \\ & \mathbf{I}_{N_c} \end{bmatrix}$, $\mathbf{H}_j$ is a Toeplitz matrix consisting of a time shifted channel impulse response in each row, $\dot{\mathbf{r}}_j$ and $\dot{\mathbf{e}}_j$ denote the time-domain received signal and additive noise, respectively.

Define a matrix $\mathbf{W}$ as

$$\mathbf{W} \triangleq \begin{bmatrix} \mathbf{A} & \mathbf{0}_{(N_p-L_h)\times(N_c-N_p+L_h)} & -\mathbf{A} \end{bmatrix},$$

where $\mathbf{A}$ is an arbitrary $(N_p-L_h)\times(N_p-L_h)$ unitary matrix. It can be easily proved that $\mathbf{W}\mathbf{H}_j\mathbf{S} = \mathbf{0}, \forall \mathbf{A}$, as long as $\mathbf{H}_j$ is Toeplitz. Therefore pre-multiplying $\dot{\mathbf{r}}_j$ by $\mathbf{W}$ removes the information bearing portion from the CP, i.e.,

$$\mathbf{y}_j \triangleq \mathbf{W}\dot{\mathbf{r}}_j = \mathbf{W}\dot{\mathbf{e}}_j. \tag{4}$$

We assume no uncoordinated interference, so that the additive noise $\dot{\mathbf{e}}_j$ is dominated by periodic impulsive noise. The periodic impulsive noise asynchronous to the main powerline frequency has a sparse power spectral density, and therefore can be decomposed in the frequency domain as

$$\dot{\mathbf{e}}_j = \mathbf{F}_N^*(\mathbf{x}_j + \mathbf{g}_j),$$

where $N = N_c + N_p - L_h$, $\mathbf{x}_j$ is a sparse vector, $\mathbf{g}_j$ captures the residual background noise and is approximated by AWGN. Defining $\mathbf{\Phi} \triangleq \mathbf{W}\mathbf{F}_N^*$ and $\mathbf{v}_j \triangleq \mathbf{W}\mathbf{F}_N^*\mathbf{g}_j$, (4) can be succinctly rewritten as

$$\mathbf{y}_j = \mathbf{\Phi}\mathbf{x}_j + \mathbf{v}_j. \tag{5}$$

Note that $\mathbf{v}_j$ is still AWGN since $\mathbf{A}$ and $\mathbf{F}_N$ are both unitary.

Suppose that before the transmission starts, the receiver has collected a few periods of noise samples using the idle intervals. it can roughly determine how to partition one period of the noise into multiple stationary intervals. Based on that information, the receiver is able to identify the OFDM symbols that are received during each stationary interval. We thereby group the corresponding measurement vectors $\mathbf{y}_j$ in the k-th stationary interval, and expand (5) into

$$\mathbf{Y}_k = \mathbf{\Phi}\mathbf{X}_k + \mathbf{V}_k. \tag{6}$$

Here $\mathbf{Y}_k$ is a matrix formed by column vectors $\{\mathbf{y}_j, \forall j \in \mathbb{S}_k\}$, where $\mathbb{S}_k$ is the index set for all OFDM symbols received in the k-th stationary interval. Similar definitions apply to $\mathbf{X}_k$ and $\mathbf{V}_k$. Note that all columns of $\mathbf{X}_k$ are sparse vectors that share an identical support. (6) is the standard multiple measurement vector (MMV) problem in compressed sensing.

The T-MSBL algorithm uses a sparse Bayesian learning (SBL) approach to solve the generic MMV problem $\mathbf{Y} = \mathbf{\Phi}\mathbf{X} + \mathbf{V}$, where $\mathbf{Y}$ is an $M \times L$ measurement matrix, $\mathbf{\Phi}$ is a known $M \times N$ dictionary matrix, $\mathbf{X}$ is an unknown $N \times L$ source matrix with each row representing a possible source, and $\mathbf{V}$ is an unknown $M \times L$ noise matrix.

The key idea is to exploit the row sparsity of the source matrix $\mathbf{X}$, and impose a sparsity promoting prior on $\mathbf{X}$ that leads to a posterior density that is concentrated over row-sparse matrices. Let $\mathbf{X}_{i\cdot}$ denote the i-th row of $\mathbf{X}$. The algorithm imposes a parameterized Gaussian prior on $\mathbf{X}_{i\cdot}$

$$p(\mathbf{X}_{i\cdot}; \gamma_i, \mathbf{B}) = \mathcal{CN}(\mathbf{X}_{i\cdot}; 0, \gamma_i \mathbf{B}), \ \forall i = 1, \cdots, N \tag{7}$$

where $\boldsymbol{\gamma} \triangleq [\gamma_1 \ \cdots \ \gamma_N]$ are nonnegative parameters controlling the row sparsity of $\mathbf{X}$, and $\mathbf{B}$ is a positive definite matrix that captures the covariance of $\mathbf{X}_{i\cdot}$. The maximum a posteriori (MAP) estimation of $\boldsymbol{\gamma}$ and $\mathbf{B}$ can be computed iteratively using the expectation maximization (EM) algorithm. Upon convergence, $\boldsymbol{\gamma}$ will become a sparse vector. To ensure a unique global solution, the number of non-zero rows in $\mathbf{X}$ has to be below a certain threshold.

A challenge in using T-MSBL to estimate noise power spectrum is that the number of peaks in $\mathbf{x}_j$ generally exceeds the threshold that guarantees a unique global solution. In that case, the EM algorithm may converge to a second global optimum $\boldsymbol{\gamma}^*$ that has a different support than that of the desired global optimum. To better guide the Bayesian inference to converge to the actual noise power spectrum, despite of its low sparsity level, we propose a more informative prior that incorporates decision feedback from the decoder.

On top of the prior (7), we impose a hyper-prior on $\boldsymbol{\gamma}$ and $\mathbf{B}$, respectively. We adopt the following conjugate priors since they generally lead to computationally tractable solutions:

$$p(\boldsymbol{\gamma}; \mathbf{a}, \mathbf{b}) = \prod_{i=1}^{N} \text{IG}(\gamma_i; a_i, b_i), \tag{8}$$

$$p(\mathbf{B}; \mu, \mathbf{\Psi}) = \text{IW}(\mathbf{B}; \mu, \mathbf{\Psi}). \tag{9}$$

Here $\text{IG}(\gamma_i; a_i, b_i)$ is the inverse Gamma distribution with the shape parameter a_i and scale parameter b_i, both of which assume non-negative values; $\text{IW}(\mathbf{B}; \mu, \mathbf{\Psi})$ denotes the inverse Wishart distribution, where $\mu > L$ is the degree of freedom and $\mathbf{\Psi}$ is a positive definite scale matrix.

Upon receiving a packet, the hyperparameters $\mathbf{a}, \mathbf{b}, \mu$ and $\mathbf{\Psi}$ are initialized with non-informative values (e.g. $\mathbf{a} = \mathbf{b} = \mathbf{0}, \mu = L+1, \mathbf{\Psi} = \mathbf{I}_L$), and are then updated iteratively based on decision feedback from the FEC decoder. In each iteration, given the hierarchical prior, the noise power estimator executes a single iteration of the EM algorithm to generate an estimate of $\boldsymbol{\gamma}$. Since $\boldsymbol{\gamma}$ is the N-point noise power spectrum, we need to compute the desired N_c-point noise power spectrum $\boldsymbol{\sigma}$ by $\boldsymbol{\sigma} = \text{diag}\left\{\mathbf{P}\mathbf{\Gamma}\mathbf{P}^*\right\}$, where $\mathbf{P} = \mathbf{F}_{N_c}\begin{bmatrix}\mathbf{0}_{N_p-L_h} & \mathbf{I}_{N_c}\end{bmatrix}\mathbf{F}_N^*$, and $\mathbf{\Gamma} \triangleq \text{diag}(\boldsymbol{\gamma})$. The diversity demodulator then combines received signals according to (3), using the current estimate of $\boldsymbol{\sigma}$ for all stationary intervals. The soft outputs, after deinterleaving, are further decoded by the convolutional decoder. In coherent mode, the receiver can use the hard decisions from

the decoder (e.g. convolutional or Reed-Solomon decoder) to reconstruct the transmitted signal, which is filtered by the estimated channel, and subtracted from the actual received signal. The residual in the frequency domain, denoted by $\hat{\mathbf{X}}'$, is an estimate of $\mathbf{X}$ and contains side information that is extracted from the redundancy of the convolutional code. Since (8) and (9) are conjugate priors, the posterior distribution of $\boldsymbol{\gamma}$ (or $\mathbf{B}$), conditioned on $\hat{\mathbf{X}}'$, is also an inverse Gamma (or inverse Wishart) distribution, with updated hyperparameters

$$\tilde{a}_i = a_i + \frac{L}{2}, \quad \tilde{b}_i = b_i + \frac{1}{2}\hat{\mathbf{X}}'_{i\cdot}\mathbf{B}\hat{\mathbf{X}}'^{*}_{i\cdot}; \tag{10}$$

$$\tilde{\mu} = \mu + N, \quad \tilde{\boldsymbol{\Psi}} = \boldsymbol{\Psi} + \sum_{i=1}^{N} \frac{\hat{\mathbf{X}}'^{*}_{i\cdot}\hat{\mathbf{X}}'_{i\cdot}}{\gamma_i}. \tag{11}$$

Note that the side information extracted from the decision feedback $\hat{\mathbf{X}}'$ is fused into the updated hyperparameters $\tilde{\mathbf{a}}, \tilde{\mathbf{b}}, \tilde{\mu}$, and $\tilde{\boldsymbol{\Psi}}$. These more informative hyper-priors are then used for noise power spectrum estimation in the next iteration. As such, we formulate a receiver that iteratively estimates noise power spectrums using decision feedback from the decoder, and uses the estimation to decode the received signal. Multiple iterations are run for every single packet. To reduce error propagation, the noise power estimation from one packet does not carry over to the next packet, i.e., the hyperparameters are re-initialized for every newly received packet. The iterative receiver structure described above is depicted in Fig. 3. Such receiver can be applied in coherent mode only, since it requires channel estimation to reconstruct the received signal from the decoder output.

Given the hierarchical prior, the MAP estimation of $\boldsymbol{\gamma}$ and $\mathbf{B}$ can be computed iteratively using the EM algorithm, following similar routines as in [17]. Please refer to [1] for derivation details. Compared to the standard T-MSBL algorithm, the update rules for $\boldsymbol{\gamma}$ and $\mathbf{B}$ now involves additional hyperparameters $\mathbf{a}, \mathbf{b}, \mu$ and $\boldsymbol{\Psi}$:

$$\gamma_i \leftarrow \frac{\hat{\mathbf{X}}'_{i\cdot}\mathbf{B}^{-1}\hat{\mathbf{X}}'^{*}_{i\cdot} + L\boldsymbol{\Xi}_{ii} + 2b_i}{L + 2a_i}, \forall i, \tag{12}$$

$$\tilde{\mathbf{B}} \leftarrow \sum_{i=1}^{N} \frac{\hat{\mathbf{X}}'^{*}_{i\cdot}\hat{\mathbf{X}}'_{i\cdot}}{\gamma_i} + \boldsymbol{\Psi}^{*}, \mathbf{B} \leftarrow \tilde{\mathbf{B}}/||\tilde{\mathbf{B}}||_{\mathcal{F}}. \tag{13}$$

Here $\boldsymbol{\Xi}$ is evaluated by (17) in [17].

IV. Simulation Results

The bit error rate (BER) performance of our proposed methods is evaluated in both synthetic and realistic periodic impulsive noise, and in CENELEC-A and FCC bands. Due to space constraints, we only present simulation results in synthetic noise and CENELEC-A band in this paper. Please refer to [1] for more comprehensive performance studies.

The synthetic periodic impulsive noise is emulated using the LPTV system model in [4], [5]. More specifically, we partition each period of the noise into three stationary intervals, covering $70\%, 29\%$ and 1% of a period, respectively. In each stationary interval, the noise is spectrally shaped using the power spectral density profile from the same field measurement in [5]. For simplicity, we assume flat channel and ideal channel estimation throughout the simulations.

We simulate the physical layer of the proposed TFMD transceiver and a reference narrowband PLC system, both of which adopt standard parameters as specified in the ITU-T G.9903 Recommendations (Table IV). Both systems can be configured to operate in either non-coherent or coherent modes, and transmit in 35.9–90.6 kHz in the CENELEC-A band. In coherent mode, for simplicity purposes we do not insert any pilots for channel estimation, since a flat channel and ideal channel estimation are assumed. As suggested by the standard, the reference system uses concatenated Reed-Solomon and convolutional coding, whole-packet interleaving, and DBPSK/BPSK modulation for improved robustness in periodic impulsive noise. On the other hand, the proposed system uses convolutional coding (i.e., with the Reed-Solomon encoder/decoder switched off in Fig. 3), a smaller interleaver across one OFDM symbol, and TFMD modulation. Since modulation diversity does not change data rates, the proposed system has a slightly higher data rates than the reference system, due to the elimination of Reed-Solomon coding. The physical layer parameters for the proposed TFMD system are outlined and compared with those of the reference system in Table IV, where a Reed-Solomon code with the input and output block lengths of k_1 and k_2 bytes, respectively, is denoted as k_2/k_1. The effective data rates, excluding the preamble and frame control header, are calculated for the coherent mode.

We adopt a Hochwald/Sweldens code with $N_d = 2$ and 3. Since each period contains a single burst that extends approximately 4 OFDM symbols, we set $\Delta T = 4$ in the time-frequency mapping. A diversity receiver with either offline or semi-online noise power estimation is used to decode the TFMD signal. The offline noise power estimation is performed once for all simulated packets, based on 10 periods of noise samples. In coherent mode, the semi-online estimator first determines the partition of stationary intervals based on 2 periods of noise samples. The entire receiver is then set to run 5 iterations for each packet.

The BER performance is evaluated for both coherent and non-coherent modes. As shown in Fig. 4, the TFMD system achieves significant performance improvement compared to the reference in both operating modes. In particular, to achieve the target BER of 10^{-4}, the TFMD system requires considerably lower E_b/N_0 than the reference system. In coherent mode, our proposed transceiver methods obtain up to 6.5 dB gain. In non-coherent mode, even larger gains (up to 8 dB in CENELEC-A) are observed. This indicates that the proposed methods are able to compensate part of the performance gap between non-coherent and coherent schemes. Increasing N_d from 2 to 3 brings additional 2–3 dB gains when the offline noise power estimator is used. Although the offline estimator consistently outperforms the semi-online alternative, it is observed that the

Parameters	Reference System	TFMD System
Sampling Frequency	400 kHz	
FFT Size N_c	256	
CP Length N_p	30	
# of Subcarriers	128	
Data Subcarriers	23–58	
Convolutional Code	rate 1/2, length 7	
Reed-Solomon Code	251/235	N/A
Interleaver Size (Bits)	4032	36
Packet Size (Bytes)	235	
Data Rate (kbps)	23.5	25

TABLE I. Physical layer parameters of the reference and proposed narrowband PLC systems.

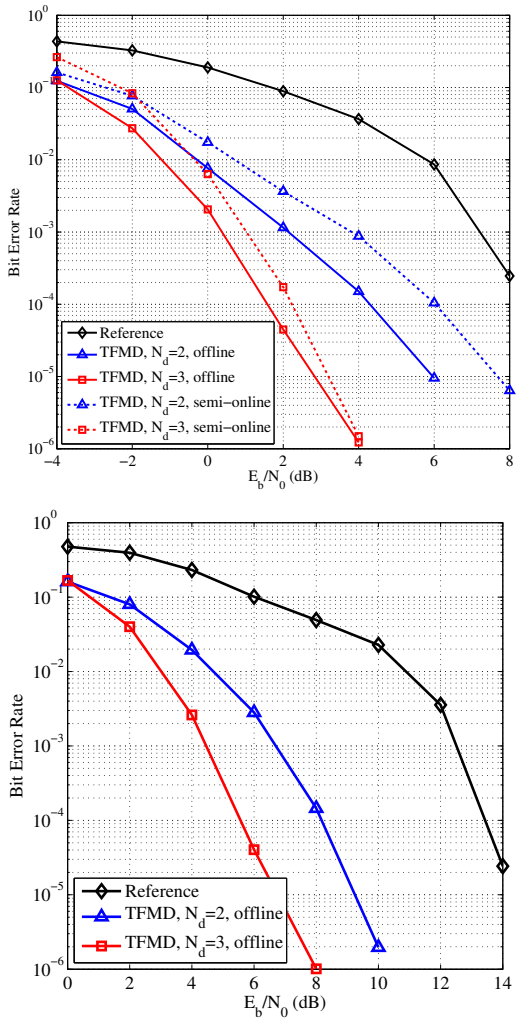

Fig. 4. Bit error rate performance of the proposed TFMD transceiver in periodic impulsive noise. Performance is evaluated for the coherent mode (top) and the non-coherent mode (bottom) in the CENELEC-A band. N_d denotes the length of modulation diversity codewords. "Offline" and "semi-online" refer to the noise power estimation algorithms.

E_b/N_0 gap between the two remains below 2 dB and becomes smaller as N_d increases. As such, in the situations where the offline noise power estimator is infeasible due to limited idle time in the shared PLC channel, the semi-online estimator can still provide significant performance improvement, especially with larger N_d.

In addition to the superior communication performance, our proposed transceiver methods can be implemented with lower or comparable complexity relative to the reference narrowband PLC system. With TFMD, the transmitter can be relieved from Reed-Solomon coding and whole-packet interleaving, both of which are known to be computationally intensive and memory consuming. It can be shown [1] that receiver complexity is much lower than (if using offline noise power estimation) or comparable to (if using semi-online noise power estimation) the polynomial complexity of the state-of-the-art Reed-Solomon decoders.

V. Conclusion

This paper proposes a time-frequency diversity modulation scheme to enhance the communication reliability of narrowband PLC systems in periodic impulsive noise. The time-frequency modulation diversity jointly encodes multiple bits to multiple PSK symbols, and allocates them to different subcarriers in various OFDM symbols. The receiver linearly combines received signals with weights inversely proportional to the sub-channel SNRs. The periodically varying noise power spectrum can be estimated before or during data transmission using sparse Bayesian learning techniques. We validate the proposed transceiver methods based on periodic impulsive noise emulated from a statistical noise model in the IEEE 1901.2 narrowband PLC standard. In the future, this work could be further extended to study the impact of frequency-selective channel on codebook design and receiver methods.

References

[1] J. Lin, T. Pande, I. H. Kim, A. Batra, and B. L. Evans, "Time-frequency modulation diversity to combat periodic impulsive noise in narrowband powerline communications," *IEEE Trans. Comm.*, under review.

[2] S. Galli, A. Scaglione, and Z. Wang, "For the grid and through the grid: The role of power line communications in the smart grid," *Proc. of the IEEE*, vol. 99, no. 6, pp. 998–1027, 2011.

[3] "G.9903 : Narrowband orthogonal frequency division multiplexing power line communication transceivers for G3-PLC networks," 2014. [Online]. Available: http://www.itu.int/rec/T-REC-G.9903

[4] "IEEE standard for low-frequency (less than 500 kHz) narrowband power line communications for smart grid applications," 2013. [Online]. Available: http://standards.ieee.org/findstds/standard/1901.2-2013.html

[5] M. Nassar, J. Lin, Y. Mortazavi, A. Dabak, I. H. Kim, and B. L. Evans, "Local utility power line communications in the 3-500 kHz band: Channel impairments, noise, and standards," *IEEE Signal Process. Magazine*, vol. 29, no. 5, pp. 116–127, 2012.

[6] M. Katayama, T. Yamazato, and H. Okada, "A mathematical model of noise in narrowband power line communication systems," *IEEE J. Sel. Areas Comm.*, vol. 24, no. 7, pp. 1267–1276, 2006.

[7] K. F. Nieman, J. Lin, M. Nassar, K. Waheed, and B. L. Evans, "Cyclic spectral analysis of power line noise in the 3-200 kHz band," in *Proc. IEEE Int. Symp. Power Line Comm. and Appl.*, 2013.

[8] J. Lin, M. Nassar, and B. L. Evans, "Impulsive noise mitigation in powerline communications using sparse Bayesian learning," *IEEE Journal on Selected Areas in Comm.*, no. 7, pp. 1172–1183, 2013.

[9] R. García, L. Díez, J. Cortes, and F. Canete, "Mitigation of cyclic short-time noise in indoor power-line channels," *Proc. IEEE Int. Symp. Power Line Comm. and Appl.*, pp. 396–400, 2007.

[10] A. Liano, A. Sendin, A. Arzuaga, and S. Santos, "Quasi-synchronous noise interference cancellation techniques applied in low voltage PLC," *Proc. IEEE Int. Symp. Power Line Comm. and Appl.*, 2011.

[11] J. Lin and B. L. Evans, "Cyclostationary noise mitigation in narrowband powerline communications," *Proc. APSIPA Annual Summit Conf.*, 2012.

[12] S. Nayyef, C. Tsimenidis, A. Al-Dweik, B. Sharif, and A. Hazmi, "Time-and frequency-domain impulsive noise spreader for OFDM systems," in *IEEE Int. Conf. on Trust, Security and Privacy in Computing and Comm.*, 2012, pp. 1856–1861.

[13] R. Schober, L.-J. Lampe, W. H. Gerstacker, and S. Pasupathy, "Modulation diversity for frequency-selective fading channels," *IEEE Trans. Info. Theory*, vol. 49, no. 9, pp. 2268–2276, 2003.

[14] J. Boutros and E. Viterbo, "Signal space diversity: a power-and bandwidth-efficient diversity technique for the Rayleigh fading channel," *IEEE Trans. Info. Theory*, vol. 44, no. 4, pp. 1453–1467, 1998.

[15] A. Batra and J. Balakrishnan, "Improvements to the multi-band OFDM physical layer," in *Consumer Comm. and Networking Conf.*, vol. 2. IEEE, 2006, pp. 701–705.

[16] B. M. Hochwald and W. Sweldens, "Differential unitary space-time modulation," *IEEE Trans. Comm.*, vol. 48, no. 12, pp. 2041–2052, 2000.

[17] Z. Zhang and B. D. Rao, "Sparse signal recovery with temporally correlated source vectors using sparse Bayesian learning," *IEEE Journal of Selected Topics in Signal Processing*, vol. 5, no. 5, pp. 912–926, 2011.